Laboratory Calibration of FOS Throughput

George Hartig
Space Telescope Science Institute

Instrument Science Report CAL/FOS-053
January 1989

Abstract

Significant changes have been made to the FOS optical and detector systems since the previous absolute throughput measurements were reported. New calibration data were obtained, in ambient, in March and August, 1988, following these modifications. While the blue side efficiencies are slightly greater than those measured in 1984, marked improvements have been made in the red side throughput, as a result of detector replacement, optical realignment, and re-coating of the collimator mirror. However, FOS model calculations continue to overpredict the throughput of both sides of the spectrograph, in a wavelength-independent manner.

I. Introduction

Extensive laboratory measurements were made during the summer of 1984 at Martin Marietta Astronautics Group, Denver, (MMAG) to determine the absolute throughput of the FOS over its entire spectral range. Although the general conclusion reached from the analysis of those data was that the FOS performed reasonably well, comparison with the predicted throughput showed a global, wavelength-independent deficiency, amounting typically to about 35% (Hartig and Bohlin, 1985). This was most easily interpretted as due to misalignment of the calibration source, the ambient or vacuum ST optical simulator (ASTOS or VSTOS). Internal vignetting, due to misalignment of the optical elements and/or baffling, was also identified as a possible explanation for the deficiency, with some contribution from degradation of the FOS optical surfaces (dust, smudges, etc.).

Later attempts to determine the source of the efficiency loss, after the FOS was shipped to Lockheed, Sunnyvale (LMSC), were inconclusive, but indicated that STOS alignment was probably not the major contributing factor and further implicated internal vignetting. Conclusive evidence was finally obtained, in April, 1987, utilizing modifications of the ASTOS to permit direct visual inspection of the optical paths. These visual mappings showed that losses of about 30% were incurred on the red side from a combination of baffle and grazing mirror misalignments. On the blue side, a bulge in the multi-layer insulation (MLI) blanket between the two upper baffles vignetted about 15% of the beam.

Following careful study of the misalignment problem and a demonstration that the FOS optics could be reasonably well aligned (both internally and with the telescope) with an adjustment of the grazing incidence mirror mount, a realignment was approved by the project office and successfully performed at LMSC in October, 1987. The baffles were also

adjusted to eliminate vignetting, and the collimator mirrors were both removed, re-coated at Goddard Space Flight Center (GSFC) with higher efficiency coatings, and reinstalled. The ASTOS was further modified, with a fixed, pinned and shimmed base, to accurately represent the beams from the telescope into each side of the FOS.

Simultaneous with the optical realignment effort, the development of a new, stable red digicon (F12) was proceeding at SAI and MMAG. This resulted in an excellent replacement detector for the F8 digicon, which was suffering continuing losses of red response. The F12 detector and the F7 blue detector (newly refurbished with many noisy charge amps replaced) were installed in the FOS in February, 1988. During the subsequent alignment process, attempts to center the blue side spectra on the detector, as required, were thwarted, apparently because of insufficient travel in the detector mount. Although this difficulty was an artifact of further optical misalignment, in this case involving a tilt error in the mounting of the the filter/grating wheel assembly (FGWA), the adopted, ready solution was to rotate the blue side collimator to effect the required image displacement. This misalignment of the collimator resulted in a small decentering of the beam at the dispersers, and a loss of a few percent in efficiency on the blue side. All of the calibration data discussed herein was obtained after the FOS side panels were reinstalled in February, 1988.

Finally, after the new stainless steel heat pipes were installed and the ultimate detector adjustments were performed, the MLI blankets were installed, with modifications to assure that no bulging that could cause vignetting would be possible. A confirmatory set of calibration data was then obtained, on 24-26 August, 1988, after the the FOS was "buttoned-up" for the last time.

II. Absolute Photometric Calibration Method

a) Test Procedure

The ambient Absolute Photometric Calibration (APC) test procedure, YCAPC2, used for the all the 1988 APC measurements, is summarized in Tables 1 and 2. About 24 spectra were obtained from each side of the FOS, each with the standard overscanning (5 diodes) and X-stepping (4). Three Y-steps were always used, such that spectra were obtained at the nominal YBASE and at positions $\pm 40\mu$ from that value, to assure full registration of the spectrum with the diode array. Spectra are obtained with each of the appropriate disperser/detector combinations, to cover the available spectral ranges above the air cutoff at about 2000Å. All data were obtained with the ASTOS, with diffuser screen #2, and its new fixed base. The primary standard source, for wavelengths above 2500Å, was the GS-180 tungsten-halogen lamp (type FEL, 1000W); a deuterium lamp, designated DL-117, was used below 2500Å, where the FEL lamp spectrum becomes too faint. Each lamp was allowed to stabilize for at least 20 minutes prior to data collection.

Scattered red light makes a significant contribution to the measured spectra of the tungsten lamp in the UV, below 3200Å. Spectra were obtained with a GG375 blocking filter, placed over the FOS entrance port on an appproximately 2 cm tall opaque cylinder, with the H27 grating and the prism, in order to estimate the count rates due to scattered red light.

Another effect that requires correction is the light loss due to diffraction at the smaller apertures. Spectra were obtained through the larger apertures for high resolution gratings, with moderate count rates. Spectra obtained through the small apertures with the same gratings permit a determination of the diffraction loss correction, as a function of wavelength, that must be applied to the low resolution (high count rate) spectra obtained through the same small apertures.

As a check that the ASTOS is properly aligned with the FOS and that there are no obstructions in the beam from the ASTOS through the FOS, spectra were also obtained with the ASTOS f/24 (centrally occulted) stop removed. Comparison of the count rates obtained with and without the stop should show an approximately 20% increase in the count rate with the stop removed, due to the removal of the central obscuration and spider and the fact that the FOS optics are nominally slightly faster than f/24. Diffraction losses through small apertures are essentially eliminated in this configuration, permitting a check on the correction for this effect.

Because of the very low dispersion of the prism at long wavelengths, its APC is particularly sensitive to errors in the wavelength calibration, such as that caused by non-repeatability of the FGWA. Internal cal lamp spectra were obtained at the same time as the prism APC spectra, without intervening FGWA rotation.

b) Related Investigations

Several additional investigations were also performed which are related to the absolute throughput determination.

1. Efficiency vs. Detector High Voltage The effective QE of the digicon detectors is somewhat dependent on the operation voltage, due to dispersion in the pulse height distribution (PHD). This effect was investigated by obtaining ASTOS/FEL lamp spectra, with several of the relevant high resolution gratings on each side, at 18kV, followed immediately by the same set of exposures at 22kV. The discriminator settings remained unchanged, but the detector pitch and YBASE values were updated between these sets. Because the exposures used for this investigation are a subset of those performed in YCAPC2, this also served as a QE repeatability check.

Figures 1 and 2 show the ratios of the count rates obtained at 22kV and 18kV measurements, for several gratings on the red and blue sides, respectively. Also shown are the manual fits which were scaled linearly to predict the quantum throughput (QT) at expected flight operation voltages from those measured at the lower voltages used for the APC. The wavelength dependence of the ratio may be a reflection of the difference in field strength at the photocathode surface, such that the low energy photoelectron escape probability is augmented at the higher voltages. The apparent upturn in the red detector ratio at short wavelengths is at least partly due to the increasing contribution of scattered red light, for which the ratio is higher than for the UV.

2. Efficiency vs. Discriminator Reference DAC Setting The digicon QE is also dependent on the level at which the lower level discriminator is set for each channel, again because of dispersion in the PHD. This effect was also investigated in March, 1988, and the results reported in CAL/FOS-050 by Cohen, et al. (1988). While the discriminator reference DAC

setting was kept at 184 for all APC exposures on both sides, this may not be the optimal value, which depends on the detector operation voltage.

Figure 3 shows the count rates obtained with the reference DAC set at several values between 124 and 204 relative to the rate at 184; an approximately linear relationship holds over this range of DAC values, with a change in QE of about .17% for each DAC unit change. A QE improvement of about 11% can be achieved by setting the reference DAC at 124, but the channel uniformity is somewhat degraded, and the detector is more susceptible to electronic noise, as is evidenced by the noise spikes in Figure 4. Tests should be made on orbit to determine the optimal compromise; operation at reduced temperature and in the electromagnetically quieter environment on orbit may permit lower DAC setting. However, if channel uniformity and noise rejection considerations require an increment (from 184) to the reference DAC setting, the FOS QT will be somewhat reduced from the levels calculated herein.

3. Scattered Room Light During the re-calibration of the ASTOS at the National Institute of Standards and Technology (NIST, formerly the National Bureau of Standards), a check was made of the amount of light contributed to the diffuser screen illumination from reflections and scattering in the room, rather than directly from the FEL lamp. This was found to be significant, and exhibited some wavelength dependence. Consequently, the NIST apparatus were configured to measure the direct illumination contribution alone. While the scattered room light contribution to the FOS measurements was expected to be somewhat smaller, since they are made in a high-bay area lacking the relatively close white ceilings of the NIST lab, the August, 1988 APC measurements included a check for this effect. A black-painted panel was held about 10 cm from the FEL lamp, to block direct diffuser screen illumination, mimicking the shutter used for the NIST calibration. Spectra obtained with and without this shutter were directly compared, showing that the scattered light contribution was indeed significant, especially at longer wavelengths. Figure 5 presents the measured indirect illumination fraction as a function of wavelength, which was used to correct the measured QT values.

4. Deuterium Lamp Repeatability The APC measurements of 1984 utilized the deuterium lamp designated DL-116. This lamp was found to be very unrepeatable, from turn-on to turn-on, in both its absolute flux output at any wavelength as well as its spectral distribution, rendering the data unusable. For this reason, the DL-117 lamp was selected for the recent measurements, and special tests were performed to determine its repeatability. Following the March APC measurements, the DL-117 lamp was turned on and spectra obtained using the H27 grating and B3 aperture on the blue side, as for the APC, on four separate occasions. After a twenty minute stabilization period, the lamp was found to be quite repeatable, matching the original spectrum within 2%, until the final measurement. This last check, made on 22 March after a 9 hr period of lamp operation (for polarizer throughput measurements) showed a wavelength-independent drop in signal of 6%. The final APC measurement made on 25 August compares within a few tenths of a percent with the 22 March measurement, and is taken to be the definitive measurement, since the ASTOS/DL-117 calibration was performed in the interim between these APC measurements, in July.

III. NIST ASTOS Calibration

The ASTOS and its associated lamps and power supplies were shipped to the NIST, Radiometric Physics Division, for absolute calibration during July 1988. The spectral irradiance at the plane of the FOS entrance apertures was determined for the GS-180 FEL lamp, over the spectral range 2500-8500Å, and for the DL-117 deuterium lamp, over the spectral range 2000-3000Å. Below 3000Å, the spectral radiance was measured and converted to spectral irradiance using the measured geometry of the ASTOS. At longer wavelengths, the irradiance was measured directly. Details of the measurement technique and results are described in the test report (Walker and Gibson, 1988).

A particularly interesting result of the ASTOS calibration is the apparent *increase* in radiance of the GS-180 FEL lamp, compared to its previous measurement in September, 1984. This brightening amounts to about 3% for wavelengths below 3000Å, increasing to about 7% at 4000Å, above which it remains constant. Although the ASTOS was reworked considerably in the interim between these calibrations, the essential parts which determine the beam geometry were unchanged, so the increase in irradiance can be ascribed only to a true brightening of the GS180 lamp or measurement error. The standard errors quoted for the NIST measurement range from 5% in the UV, to 3% in the visible, for this lamp. An increase in the actual lamp operation electrical current cannot be responsible for the brightening since this would raise the UV flux more than that in the visible, the opposite of what is observed. Furthermore, although the contribution to the ASTOS irradiance from light scattered from surrounding surfaces has a character similar to the observed brightening in both magnitude and spectral distribution, it is unlikely that this is the source of the observed increase in irradiance, since special care was used to subtract the indirect illumination contribution in the current measurements, whereas this was *not* attempted in 1984.

IV. Data Reduction

The data obtained in March were compared with those of August, to determine the degree of repeatability, to ascertain that the ASTOS irradiance and alignment with respect to the FOS remained stable, and to assure that the FOS response was not changed as a result of the detector removal and realignment, and MLI blanket and flight panel installation that ensued in the interim. The GS-180 lamp data for each of the high resolution gratings were directly compared; no deviations in the August/March raw count ratios greater than 2% were discovered, when the data were properly selected to include only YSTEPs well registered with the diode array. The remaining discrepancies may be due to spatial non-uniformity of the photocathode response (since the spectra were imaged to slightly different portions of the photocathodes in March and August), and small losses due to residual misalignment with the diode array (exacerbated by detector distortion and theta-Z alignment error). The DL-117 lamp measurement of the H27 grating on the Blue side in August repeated nearly perfectly the final March measurement, as discussed above (§IIb-4). All indications are that the August data, combined with the July ASTOS calibration, are truly representative of the current throughput of the FOS; these data alone were further analyzed as follows.

The APC data were reduced using an IDL program (APC.PRO), which includes the following steps:

1. The raw data are corrected for disabled channels and digicon non-linearity, and a wavelength scale computed, with routine YREDUCE.
2. The three Y-steps are compared to determine which step(s) are fully registered with the diode array; the valid spectra are added and the count rates calculated. In some cases, poor registration of the spectra with the array required that different portions of two of the Y-steps be coadded.
3. A background contribution, determined from the special observations made with cut-off filters for the H27 and PRISM spectra of the tungsten lamp, or otherwise deduced from portions of the spectrum below the internal blocking filters (L65) or air cut-off, are subtracted from the measured count rates.
4. The wavelength interval covered at each pixel is calculated and the source irradiance at the mean wavelength is interpolated from the NIST calibration data.
5. The entrance aperture area, from the microscope measurements presented by Lindler, Bohlin, and Hartig (1985), is used to calculate the flux (photons s^{-1} $Å^{-1}$) entering the FOS. The microscope determinations of aperture area are used, rather than the subsequent measurements using the ASTOS to determine relative flux transmission, because the latter are affected by aperture diffraction losses. The area of the A4 lower aperture on the red side, which is known to be significantly larger now than it was originally when the microscope measurements were made, was estimated by comparison of H27 grating spectra obtained through the A4 and B3 apertures, with the ASTOS stop removed. The diffraction loss for these configurations is minimal. The area was determined to be $1.02 \cdot 10^{-5}$ cm^2, corresponding to a 31.9μ square aperture.
6. The throughput is calculated for each pixel, then interactively smoothed and resampled.

The resulting raw QT must then be corrected for small aperture diffraction losses and scattered light from the room onto the ASTOS diffuser screen, and converted to the expected QT at the nominal operation voltage, as indicated in sections II.b)1-3 above.

Diffraction losses, as a function of wavelength, were estimated for all aperture/side configurations utilized in the APC, using a program which calculates the Fraunhofer diffraction pattern at the collimator plane due to the aperture for each of the incident beam directions into which the f/24, centrally occulted, ASTOS beam was artifically divided. This model is normalized, by adjusting the effective collimator radius, to the APC data obtained for this purpose (cf.§II.a). The adopted collimator radii are: 22.6 and 21.5 mm, for the red and blue sides; these are quite reasonable since the specified clear aperture is 21.5 mm and the outside radius is 23.0 mm. The diffraction losses, as the percentage of beam falling outside the effective collimator radius as a function of wavelength, are presented in Figure 6. The slightly smaller effective radius of the blue collimator, and consequently larger diffraction loss, is indicative of the residual optical misalignment on that side.

The standard wavelength calibration, derived from data obtained with other procedures (Kriss, et al. 1988), is sufficiently accurate for APC reduction for most dispersers. However, the low dispersion of the prism requires the use of special internal cal lamp data, obtained with the APC spectra, to adjust the standard wavelength scales. The adjustment was achieved by determining a (constant) offset using a simple cross-correlation of each APC prism cal lamp spectrum with that used for the wavelength calibration, and modifying the X0 value in the dispersion coefficient file accordingly.

The final QT curves for each relevant disperser/detector combination are plotted in Figure 7. These represent our best current estimates of the FOS QT at the expected flight operation voltages (22.1kV and 23.1kV, for the red and blue sides, respectively) and with the discriminator REFDAC set to 184.

V. Discussion of Results

a) Comparison with Previous Results

Comparison of the QT curves presented in Figure 7 to those derived from the 1984 calibration (Hartig and Bohlin, 1985; Figures 3.1-3.4) shows a marked improvement, for all dispersers, on the red side, and a slight increase on the blue side. These results are qualitatively consistent with expectations, based on the directly observed reduction of beam vignetting and reported detector QE improvements on the red side, and increased reflectivity of both collimators resulting from their recoating.

b) Comparison with FOS Model

Figures 8 and 9 show the ratio of the measured QT to that predicted by the product of all the individually measured component efficiencies, as produced by the FOS simulator (FOSSIMX). The low resolution disperser QT ratios are shown as dashed lines, while the high resolution grating values are indicated with solid lines. A description of the component measurements is given in CAL/FOS-016 (Hartig and Bohlin, 1985); these have been updated with GSFC measurements of the new collimator coatings (performed on witness flats coated with the collimators) and new QE measurements for the replacement red detector, as provided by EVSD/SAIC and Dr. E. Beaver.

For all dispersers, the measured QTs fall well below those predicted by the model calculations, with a nearly wavelength-independent ratio of about 60%, on both sides. This ratio is very similar to those reported by Hartig and Bohlin (1985), following the 1984 QT calibrations. Although considerable improvement in throughput has been achieved in the interim, especially on the red side, the efficiency increase is not reflected in the comparison with the model predictions. The wavelength and disperser independence of the discrepancy suggests a systematic error in either the QT measurements (including the ASTOS calibration) or the model data (component efficiency measurements). The discrepancy cannot be ascribed to internal vignetting or ASTOS misalignment, since the ASTOS beams through the FOS were visually examined and seen to be properly filling the optics prior to the March APC measurements.

The drop in the measured/model QT ratio at the shortest wavelengths in Figures 8 and 9, seen in the H19, H27 and L15 curves, is not necessarily indicative of reduced UV efficiency at shorter wavelengths, e.g., as a result surface contamination. The same drop was measured in the 1984 APC, and is apparently the result of an overestimation of the model QT at wavelengths between about 1800 and 2300Å. Below 1800Å, the 1984 QT ratio recovers considerably, failing to mimic the model-predicted dip in QT around 1650Å. At still shorter wavelengths, the 1984 ratio remained similar to that measured in the near UV and visible.

c) Extrapolation to the Vacuum UV

Although the latest APC data were limited to wavelengths above the air cut-off (>2000Å), the measured QT curves can provide an indication of the far UV QTs, when used in conjunction with the FOSSIMX model calculations. For the H19 and L15 gratings this was achieved by plotting the ratio of the current QT measurement to the current model QT, along with the previous vacuum UV measurement/model ratio, normalizing the latter to the former by direct comparison over the spectral range in which they overlap, and applying the normalized ratio to the new model QT predictions. The shape of the new and old measurement/model curves are in reasonable agreement, especially for the blue side; greater differences on the red side are attributed to the change in detector and the different coating type applied to the red collimator. Since no portion of the H13 grating range could be measured in air, the previous model derating curve, *i.e.*, the wavelength-dependent factor used to reconcile the 1984 APC measurements with the model, was adjusted according to the mean normalization required for the H19 and L15 gratings on the blue side. This procedure may result in a slight underestimate of the true efficiency, since the new collimator coating is expected to improve the far UV performance more than that at the longer wavelengths.

The results are displayed in Figure 10, for the H13, H19 and L15 gratings; these represent our best current estimates of the FOS throughput for the FUV configurations.

VI. Conclusions

The FOS throughput has been increased very significantly on the red side, as a result of the replacement of the F8 detector with F12, and the optical realignment which was undertaken at LMSC during 1987. In the near UV, the QT has increased by a factor of approximately 60%, while the sensitivity at Hα has improved by a factor of more than 3, and the usable range (QT >.1% with H78 grating) has been extended to beyond 8400Å, whereas the F8 detector limit was about 7300Å in 1985, and steadily declining with time. The F12 detector shows no indications of red response degradation: QT measurements made in August, 1988 show no significant deviation from those made in March, 1988.

Although the blue side efficiencies reported here are only slightly improved over those resulting from the 1984 APC, the recoating of the collimator is expected to produce a more marked improvement in the vacuum UV, where the blue side is most useful. Furthermore, the rework of the MLI blanket performed in August 1988 will prevent future beam vignetting by blanket bulges, as observed on the blue side in March 1987.

The discrepancy between the FOS model QT predictions and the end-to-end measured efficiencies remains at about the same levels as reported by Hartig and Bohlin, based on the 1984 APC measurements. While some degradation from the original component efficiency measurements might be expected at the level of about 5% per optical surface, especially since visual examination has shown that the optics are not particularly clean, minor surface degradation cannot fully account for the discrepancy: an additional 20-30% difference in efficiency remains to be identified.

References

Cohen, R., Beaver, E. and Tudhope, D. 1988. *FOS Discriminator Settings* CAL/FOS-050.

Hartig, G. and Bohlin, R. 1985. *The Laboratory Absolute Photometric Calibration of the FOS* CAL/FOS-016.

Kriss, G., Blair, W., and Davidsen, A. 1988. *Revised FOS Wavelength Calibration* CAL/FOS-054.

Lindler, D., Bohlin, R. and Hartig, G. 1985. *FOS Entrance Aperture Sizes* CAL/FOS-019.

Walker, J. and Gibson, C. 1988. **Report of Test:** 534/241936-88. U.S. Dept. of Commerce, National Institute of Standards and Technology, September 21, 1988.

Table 1
FOS Red Side APC Exposures

Disperser	Aperture	ASTOS	Lamp	Filter	Pk cts/s	Expo (s)
H40	B1 (0.5)	f/24	GS-180	none	7000	3
H78	B1 (0.5)	"	"	"	18000	2
H78	B3 (1.0)	"	"	"	46000	10[b]
H27	B3 (1.0)	"	"	"	2000	10
H57	B1 (0.5)	"	"	"	14000	2
H57	A4 (0.1-L)	"	"	"	800	10
H40	A4 (0.1-L)	"	"	"	400	20
L65	A4 (0.1-L)	"	"	"	5000	5
PRI	A4 (0.1-L)	"	"	"	36000	1
PRI	A4 (0.1-L)	"	"	"	36000	10[a]
PRI	A4 (0.1-L)	"	INT/DIR	"	61000	1
PRI	A4 (0.1-L)	"	GS-180	GG395	35000	10[a]
H27	B3 (1.0)	"	"	"	20	15
H27	B3 (1.0)	open	"	none	2400	10
H57	B1 (0.5)	"	"	"	17000	2
H40	B1 (0.5)	"	"	"	8500	3
H78	B1 (0.5)	"	"	"	21000	2
L65	A4 (0.1-L)	"	"	"	7000	5
PRI	A4 (0.1-L)	"	"	"	42000	1
PRI	A4 (0.1-L)	"	INT/DIR	"	61000	1
H27	B3 (1.0)	f/24	DL-117	none	100	50
H19	B3 (1.0)	"	"	"	70	70
L15	B3 (1.0)	"	"	"	300	50
PRI	B3 (1.0)	"	"	"	1200	25

[a] Multiple wrap-around will occur at long wavelength; this exposure is intended to produce reasonable counts at short wavelengths.
[b] Multiple wrap-around will occur at short wavelength; this exposure is intended to produce reasonable counts at long wavelengths.

Table 2
FOS Blue Side APC Exposures

Disperser	Aperture	ASTOS	Lamp	Filter	Pk cts/s	Expo (s)
H27	B3 (1.0)	f/24	GS-180	none	1600	15
H27	B2 (0.3)	"	"	"	130	40
H40	B2 (0.3)	"	"	"	750	30
H40	B1 (0.5)	"	"	"	2300	10
L65	B2 (0.3)	"	"	"	3200	10
H57	B2 (0.3)	"	"	"	1100	20
H57	B1 (0.5)	"	"	"	3300	7.5
H57	A4 (0.1-L)	"	"	"	165	30
PRI	A4 (0.1-L)	"	"	"	3900	10
PRI	A4 (0.1-L)	"	INT/DIR	"	15000	1
PRI	B2 (0.3)	"	GS-180	"	36000	10[a]
PRI	B2 (0.3)	"	"	GG395	34000	10[a]
H27	B3 (1.0)	"	"	"	20	30
H27	B3 (1.0)	open	"	none	1900	15
H57	B1 (0.5)	"	"	"	3700	7.5
H40	B1 (0.5)	"	"	"	2600	10
L65	B2 (0.3)	"	"	"	4000	10
PRI	A4 (0.1-L)	"	"	"	4800	10
PRI	A4 (0.1-L)	"	INT/DIR	"	15000	1
H27	B3 (1.0)	f/24	DL-117	none	70	75
H19	B3 (1.0)	"	"	"	60	75
L15	B3 (1.0)	"	"	"	250	20
PRI	B3 (1.0)	"	"	"	800	25

[a] Multiple wrap-around will occur at long wavelength; this exposure is intended to produce reasonable counts at short wavelengths.

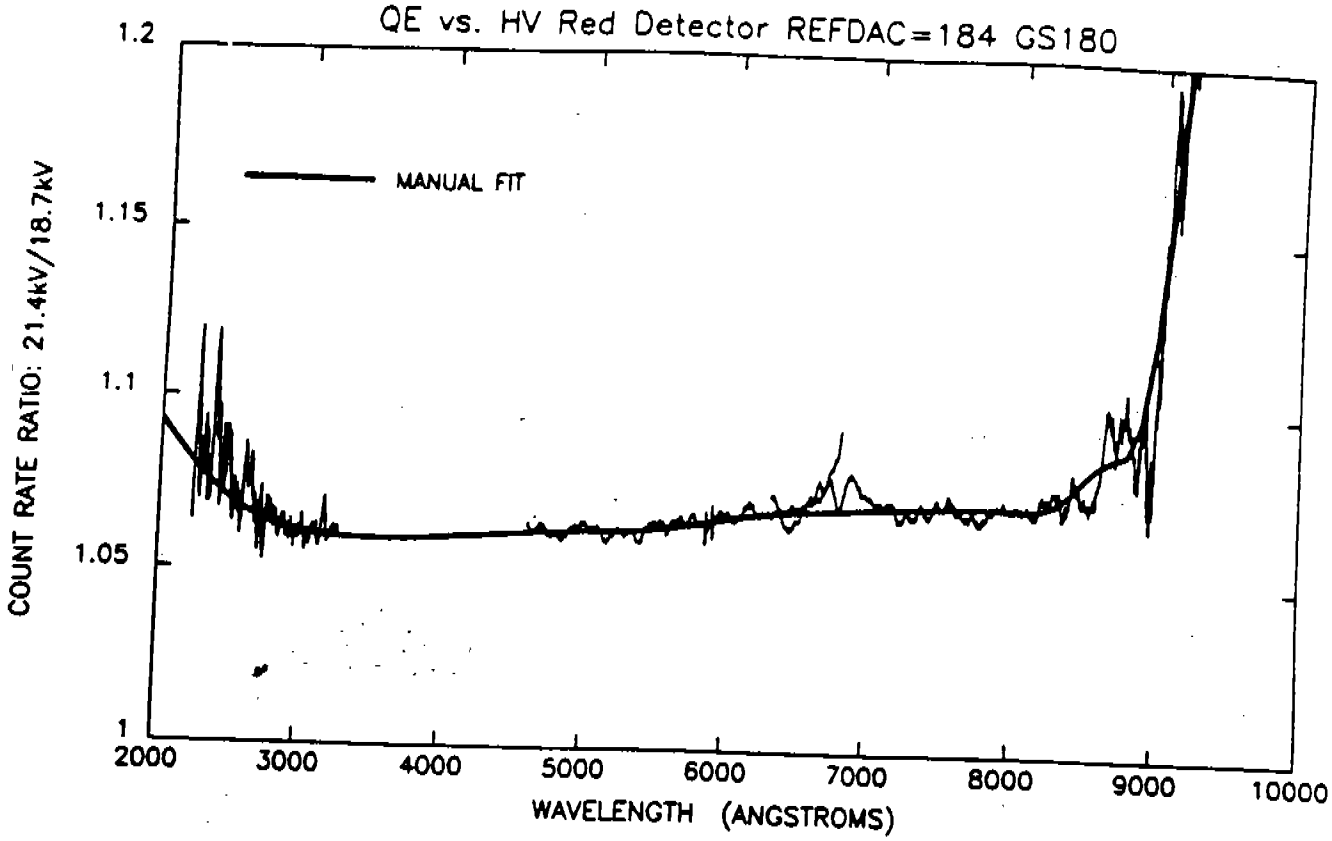

Figure 1. Paired-pulse corrected count rate ratio for red detector operation at 21.4 and 18.75kV, as a function of wavelength. The H27, H57 and H78 gratings were used with the ASTOS tungsten-halogen lamp to obtain these data.

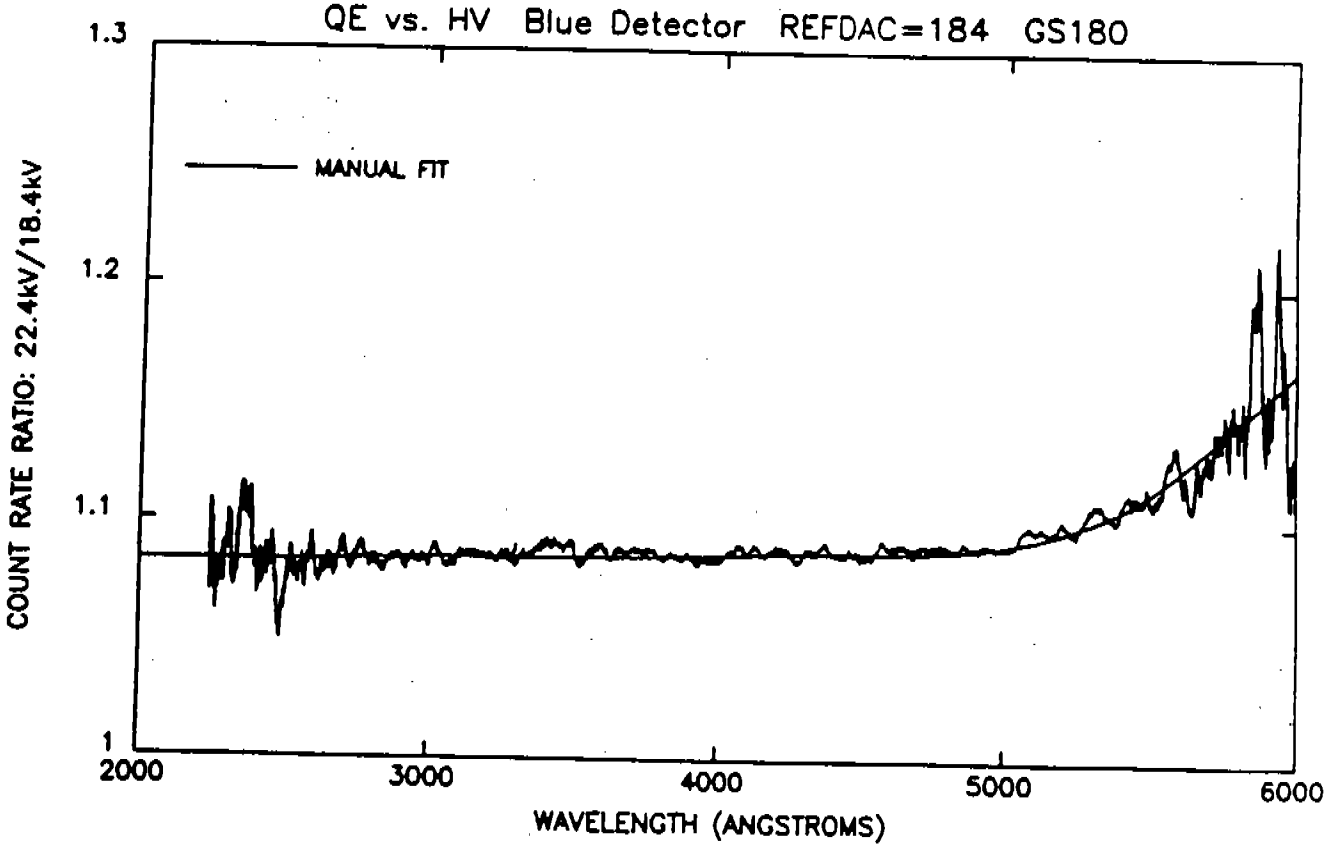

Figure 2. Paired-pulse corrected count rate ratio for blue detector operation at 22.4 and 18.4kV, as a function of wavelength. The H27, H40 and H57 gratings were used with the ASTOS tungsten-halogen lamp to obtain these data.

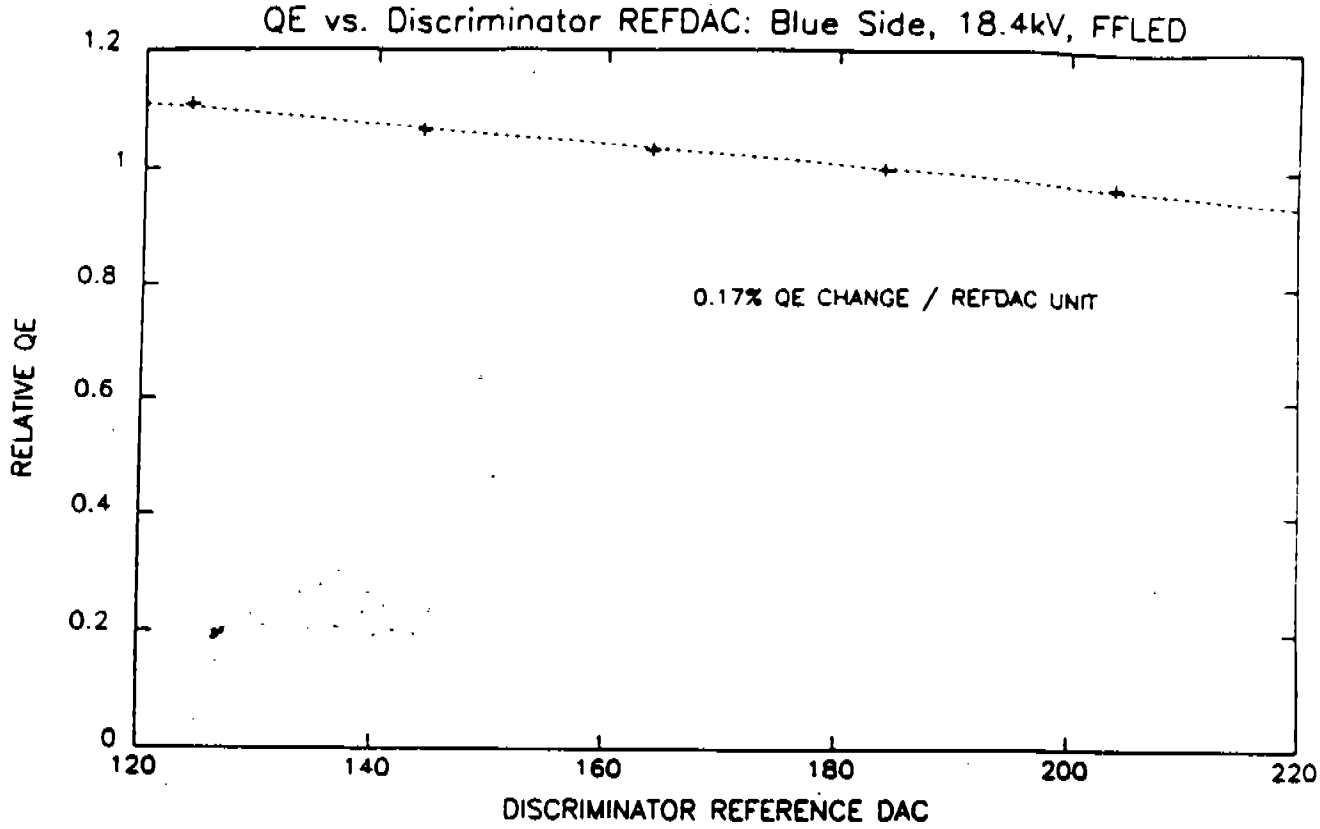

Figure 3. Relative quantum efficiency of the blue detector as a function of discriminator reference DAC setting, at 18.4 kV. The flat-field LED was used for direct detector illumination. A linear fit serves as a reasonable approximation to the observations over the measured DAC range.

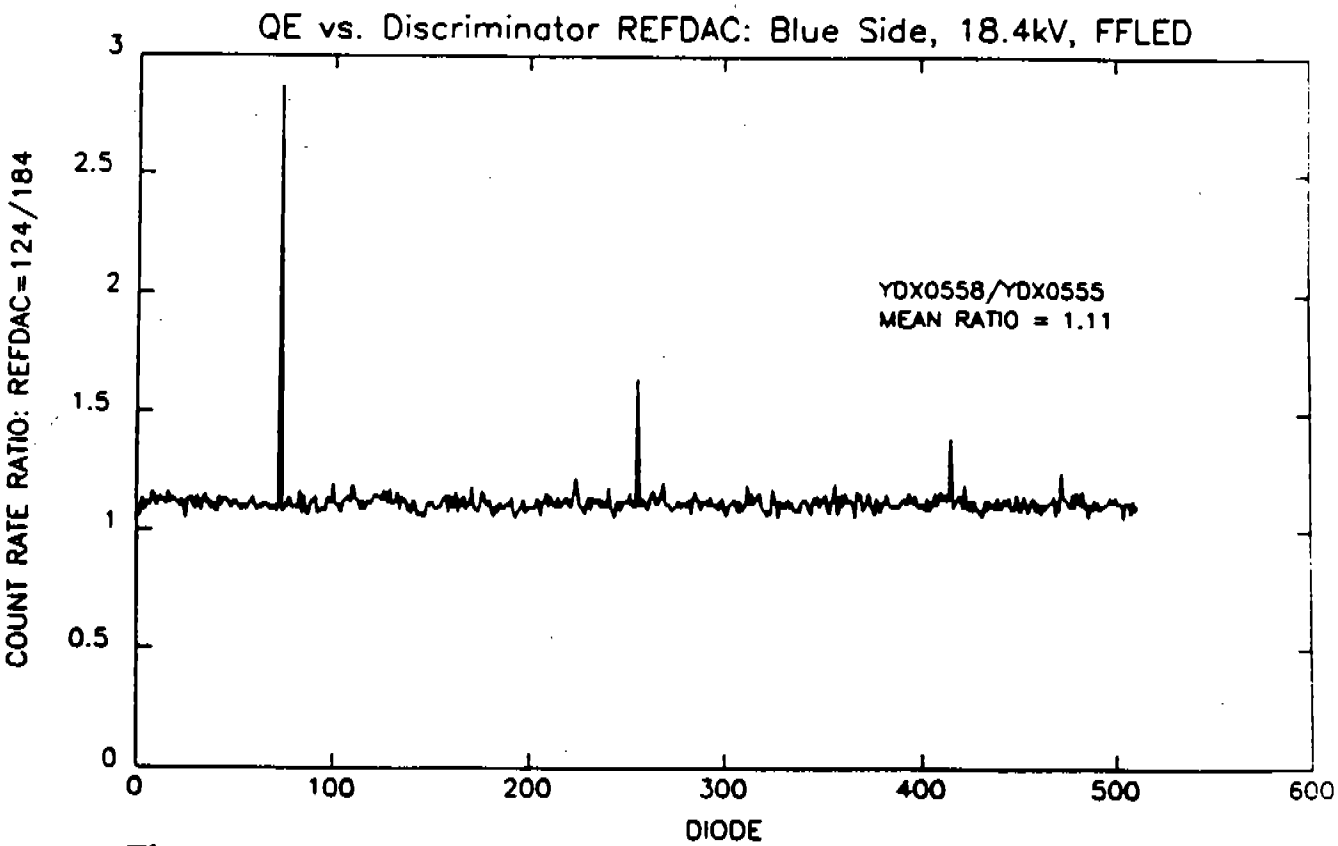

Figure 4. Count rate ratio for the flat-field LED illuminated blue detector at discriminator reference DAC settings of 124 and 184. Although the effective quantum efficiency is increased by 11% by lowering the discriminator level, the detector suffers considerably less noise immunity, as evidenced by the spikes due to channels which became noisy at the lower DAC value.

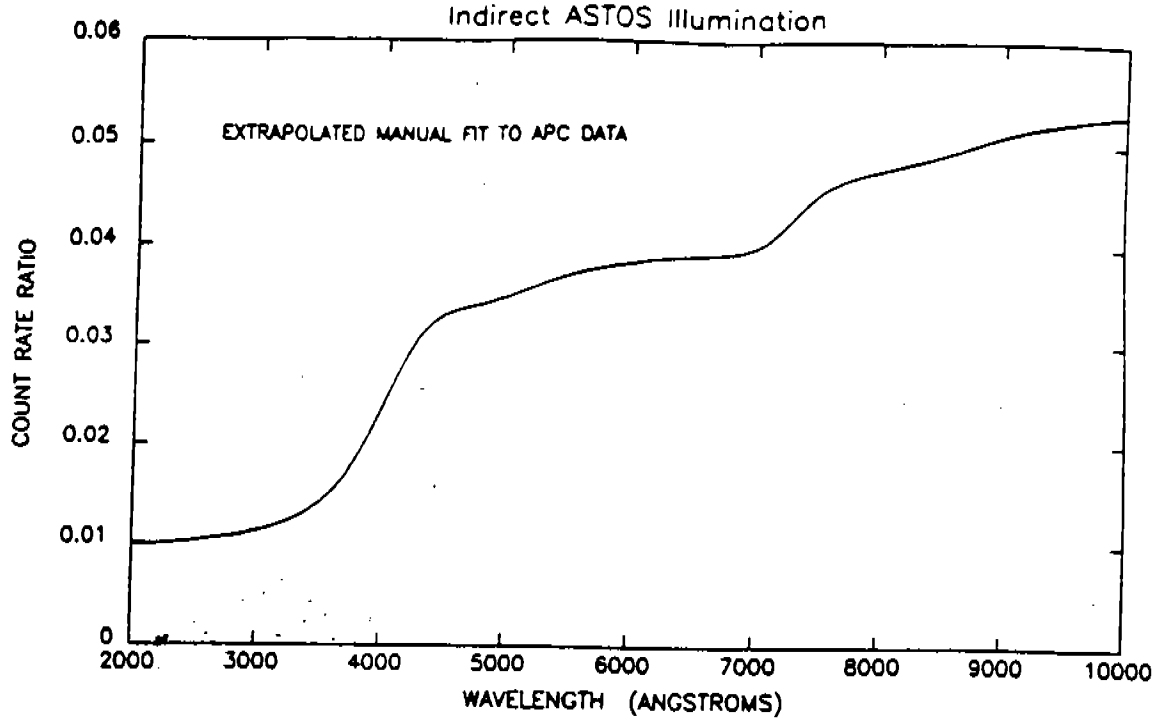

Figure 5. Count rate ratio, as a function of wavelength, with the direct beam path from the tungsten-halogen lamp to the diffusing screen blocked with a black shutter and unblocked (normal configuration). Light scattered from surfaces in the surroundings makes a significant, but correctable, contribution to the ASTOS irradiance at the FOS apertures. Data were obtained with the H40 and H78 gratings on the red side, and the H57 grating on the blue side, and an extrapolated manual fit used to correct the APC results.

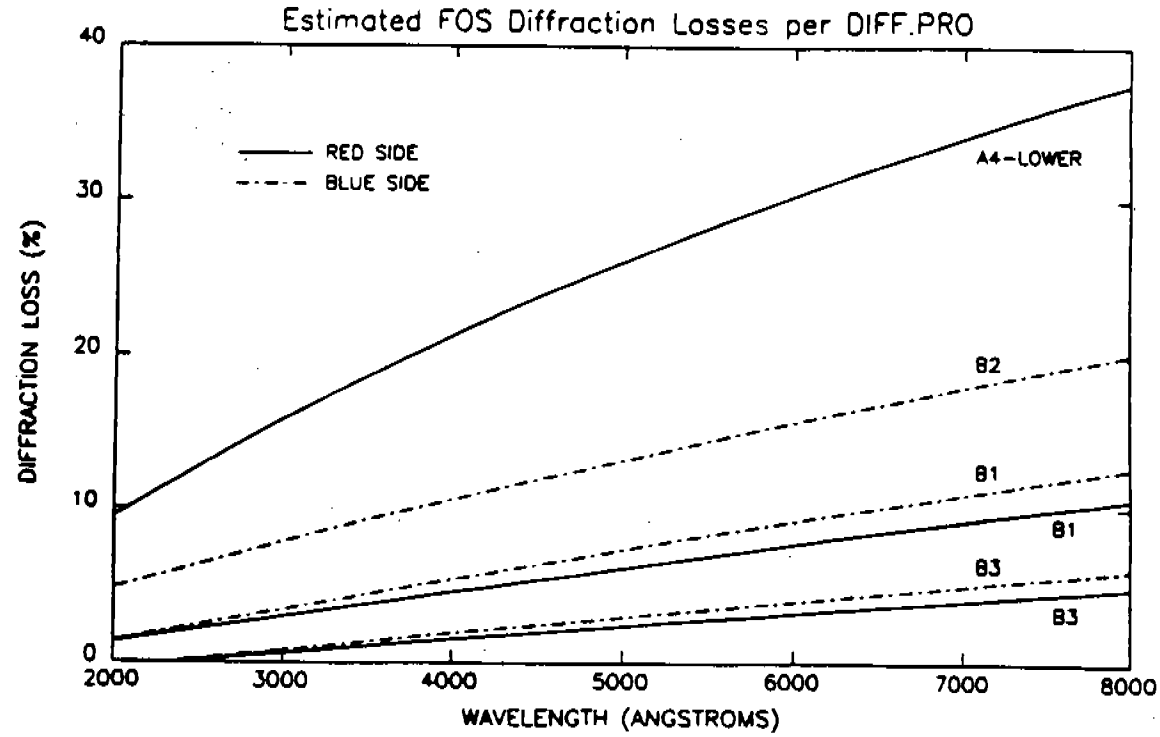

Figure 6. Diffraction losses, as a function of wavelength, for each of the pertinent aperture/side combinations. The blue side effective collimator radius (outside which diffracted light is lost) is somewhat smaller than that of the red side, resulting in slightly larger losses for the same aperture sizes.

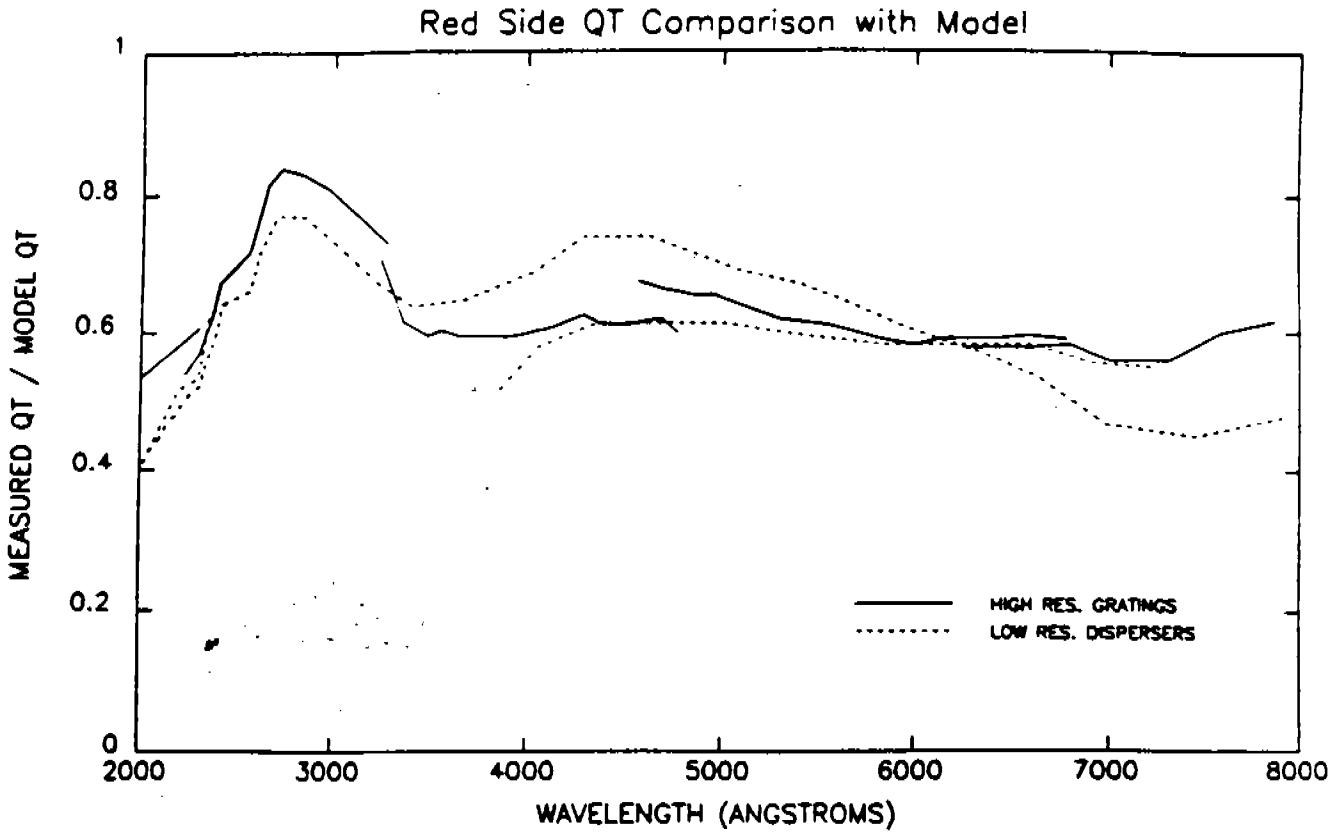

Figure 8. Comparison of the red side APC results of Figure 7 with the FOS model efficiency calculations, based on individual component efficiency measurements. The high resolution gratings are shown as solid curves, low resolution dispersers are dashed curves. The model continues to overpredict the FOS throughput measurements, in an manner that is approximately independent of wavelength and disperser.

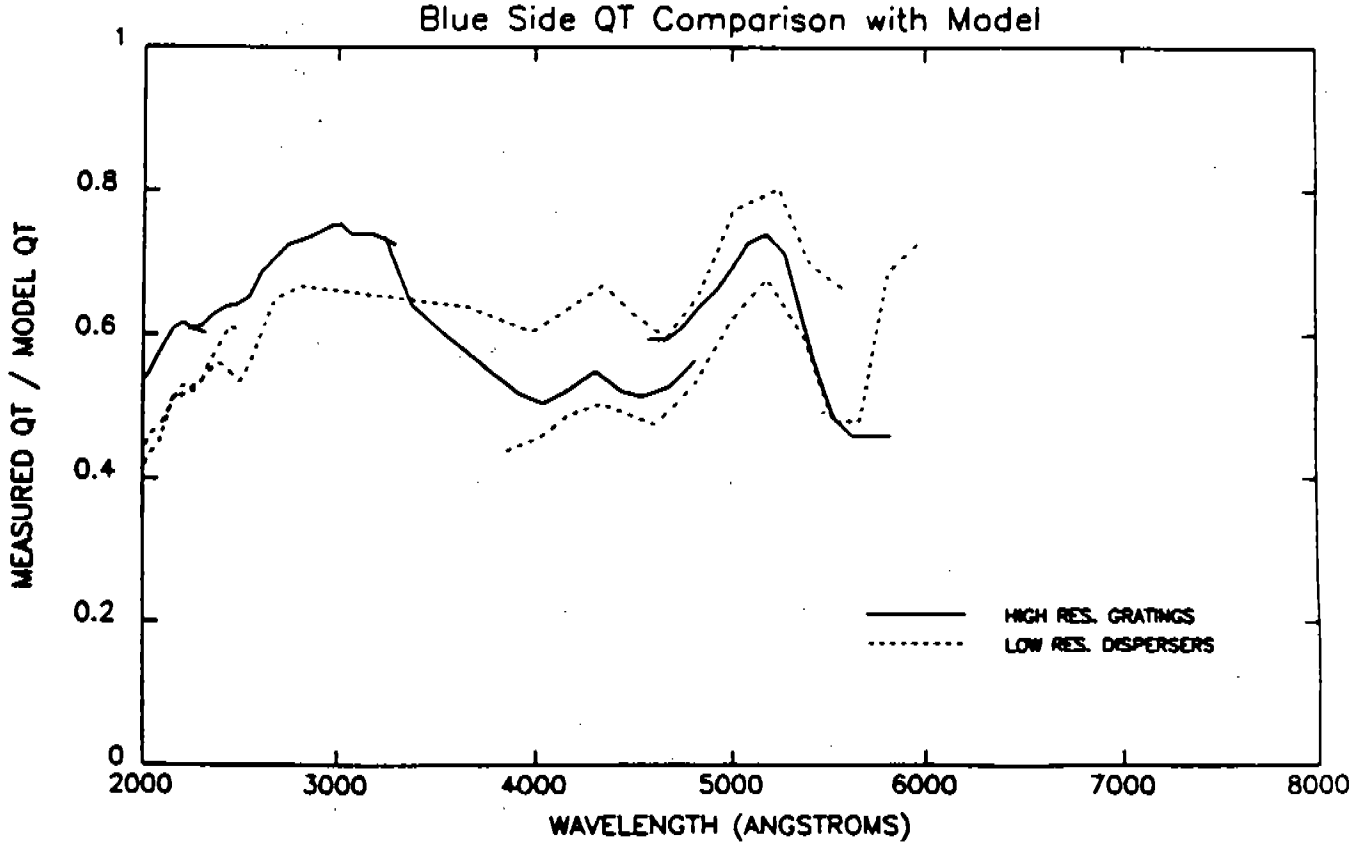

Figure 9. Comparison of the blue side APC results of Figure 6 with the FOS model efficiency calculations, as in Figure 7.

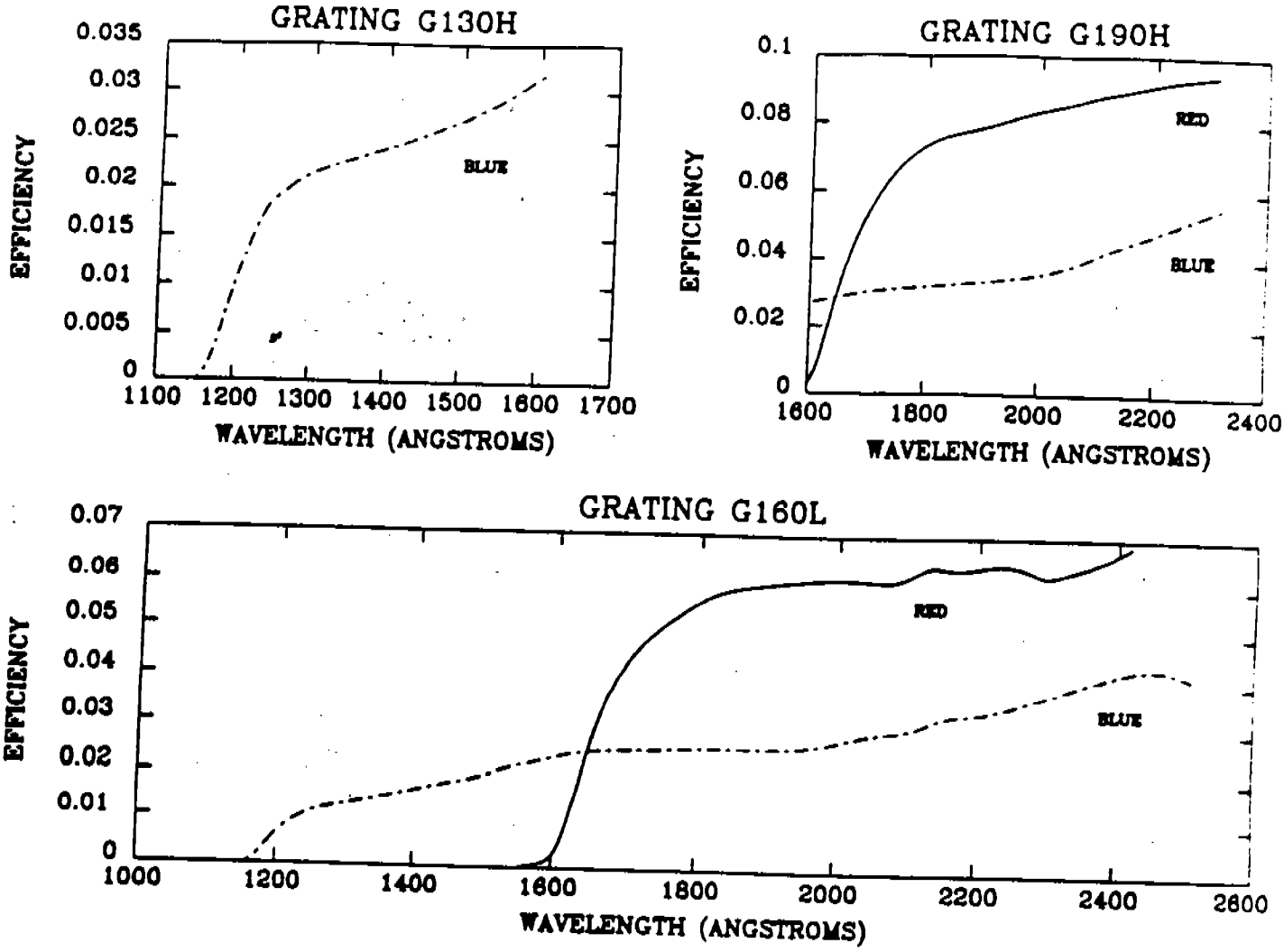

Figure 10. FOS efficiencies for the far UV dispersers. The throughput measured above 2000Å for the H19 and L15 gratings is extrapolated into the far UV using normalized model calculations. The red side efficiencies fall below those for the blue side only at wavelengths below the red detector window cut-off at about 1650 Å. The H13 grating efficiencies for the blue side are predicted with the model.

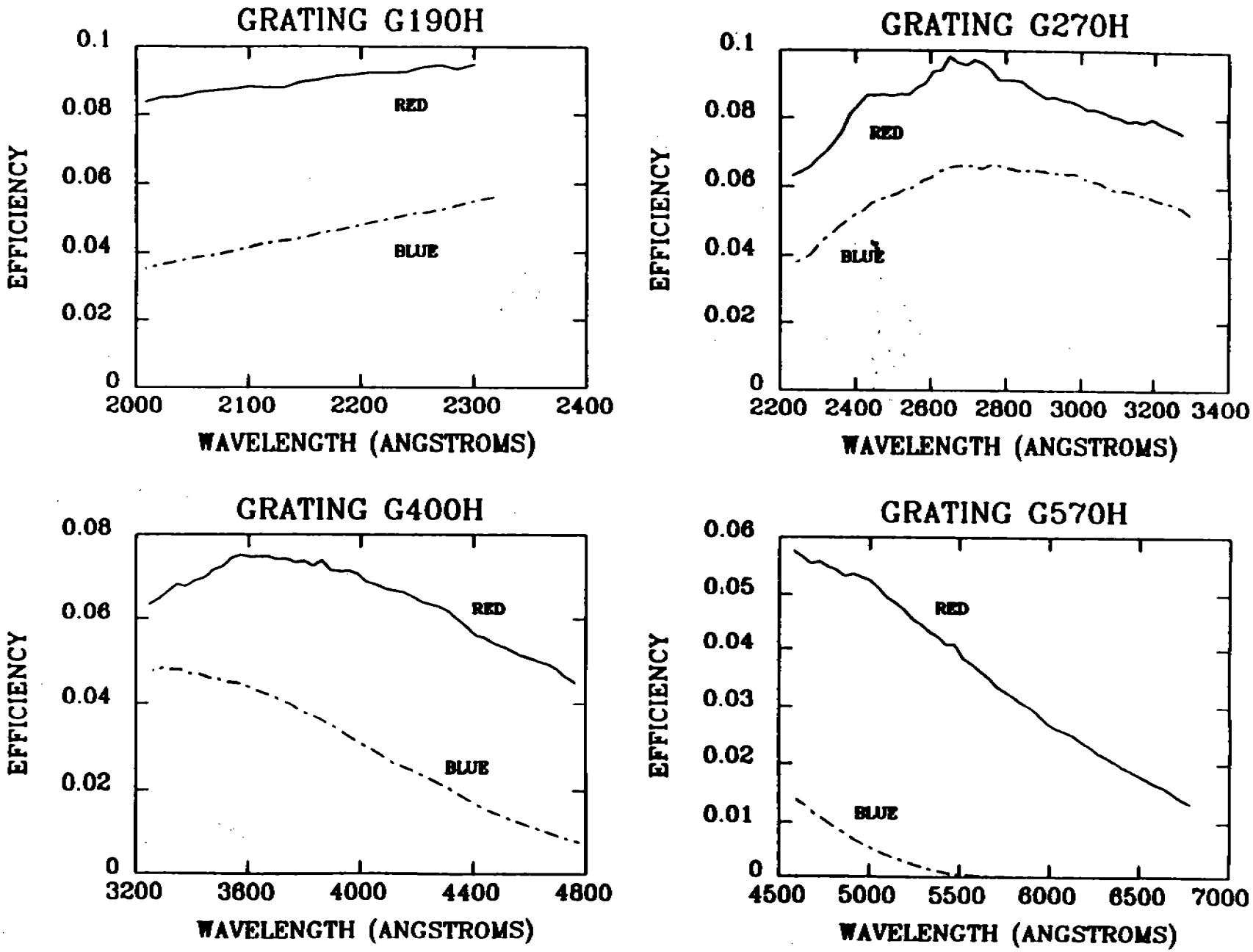

Figure 7. Corrected FOS throughput, as a function of wavelength, for each of the disperser/detector combinations measured in the ambient APC. The red side results are shown as solid curves, blue side results with dot-dash curves. The red side is seen to be considerably more efficient than the blue side for all measured wavelengths. These efficiencies are for the FOS alone, and do not include the expected losses at the entrance apertures.

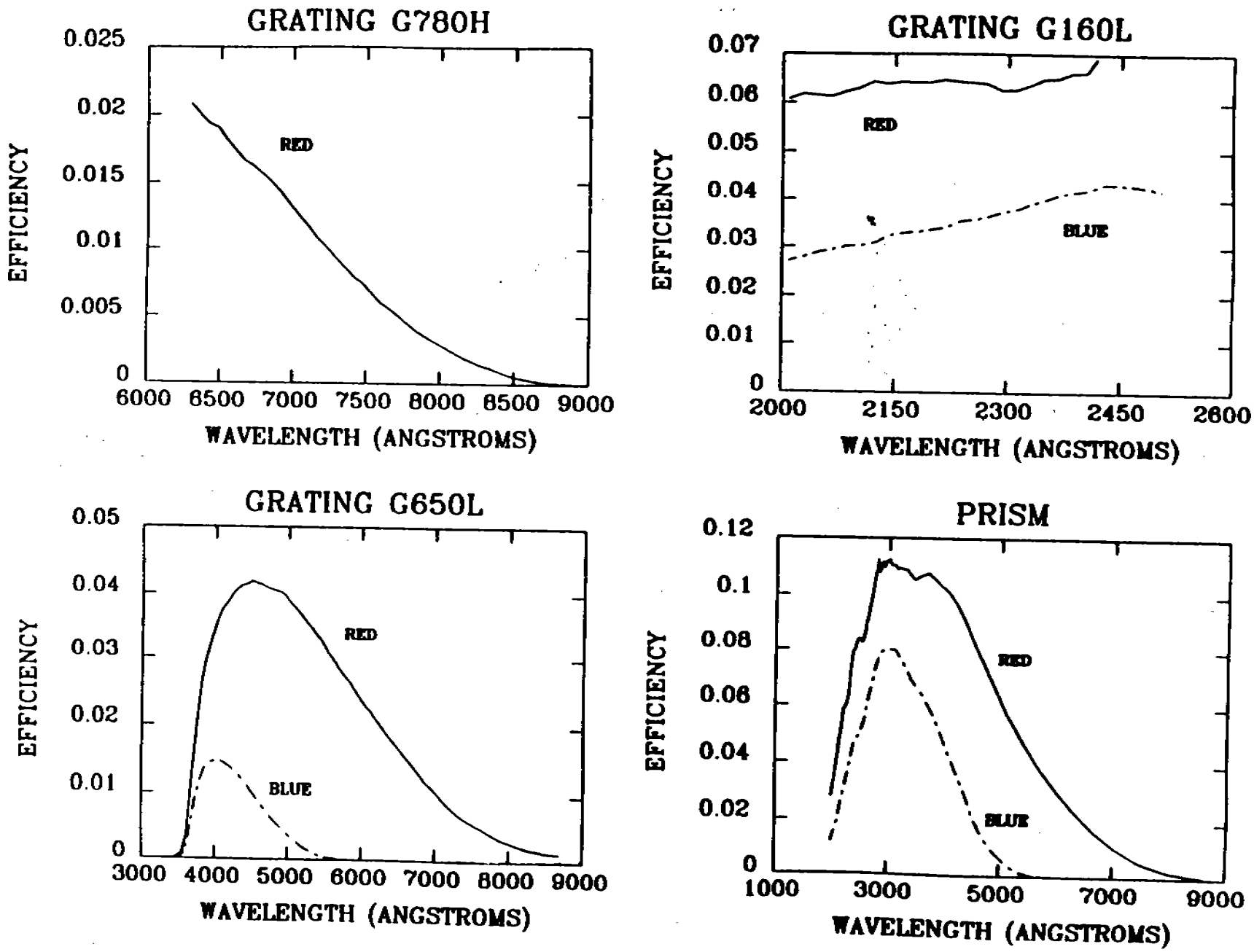

Figure 7. continued. Corrected throughput measurements for FOS alone.